






## C-halogen...O supramolecular synthons: in situ cryocrystallisation of 1,2-dihalotetrafluoroethane/HMPA adducts

Federica Bertolotti, Gabriella Cavallo, Pierangelo Metrangolo, Susanta K. Nayak, Giuseppe Resnati & Giancarlo Terraneo


To cite this article: Federica Bertolotti, Gabriella Cavallo, Pierangelo Metrangolo, Susanta K. Nayak, Giuseppe Resnati & Giancarlo Terraneo (2013) C-halogen...O supramolecular synthons: in situ cryocrystallisation of 1,2-dihalotetrafluoroethane/HMPA adducts, *Supramolecular Chemistry*, 25:9-11, 718-727, DOI: [10.1080/10610278.2013.822974](https://doi.org/10.1080/10610278.2013.822974)

To link to this article: <http://dx.doi.org/10.1080/10610278.2013.822974>



 View supplementary material 

 Published online: 25 Aug 2013.

 Submit your article to this journal 

 Article views: 103

 View related articles 

 Citing articles: 4 View citing articles 

## C–halogen··O supramolecular synthons: *in situ* cryocrystallisation of 1,2-dihalotetrafluoroethane/HMPA adducts

Federica Bertolotti<sup>a</sup>, Gabriella Cavallo<sup>b\*</sup>, Pierangelo Metrangolo<sup>b</sup>, Susanta K. Nayak<sup>b</sup>, Giuseppe Resnati<sup>b</sup> and Giancarlo Terraneo<sup>b\*</sup>

<sup>a</sup>Department of Chemistry, Università di Torino, via Pietro Giuria 7, I-10125 Torino, Italy; <sup>b</sup>NFMLab, Department of Chemistry, Materials, and Chemical Engineering “Giulio Natta”, Politecnico di Milano, via L. Mancinelli 7, I-20131 Milan, Italy

(Received 31 May 2013; final version received 2 July 2013)

The *in situ* cryocrystallisation technique has been used to obtain four adducts between hexamethylphosphortriamide and 1,2-dihalotetrafluoroethanes having iodine, bromine and chlorine as halogen-bonding donor atoms. These systems allowed for a precise comparison of different C–X··O synthons. The effectiveness and reliability of the pharmacologically important C–Cl··O synthons are proven.

**Keywords:** *in situ* cryocrystallisation; halogen bond; hexamethylphosphortriamide; halofluoroalkanes

### 1. Introduction

The halogen bond (XB) has emerged as an effective and useful non-covalent interaction of wide use in several fields of supramolecular chemistry (1). An IUPAC project has recently proposed that ‘a halogen bond occurs when there is evidence of a net attractive interaction between an electrophilic region associated with a halogen atom in a molecular entity and a nucleophilic region in another, or the same, molecular entity’ (2). The electrophilic region results from the anisotropy of the halogen’s charge distribution and is usually labeled as ‘ $\sigma$ -hole’ (3). The more polarisable the halogen atom is, the more positive the potential of the  $\sigma$ -hole. The nucleophilic region, i.e. the halogen bonding acceptor, is typically a lone pair possessing atom (e.g. the N atom of a pyridine or an amine, the O atom of a carbonyl group), a  $\pi$  system (e.g. a double or triple bonds, an arene moiety) or an anion (e.g. a halide or an oxyanion).

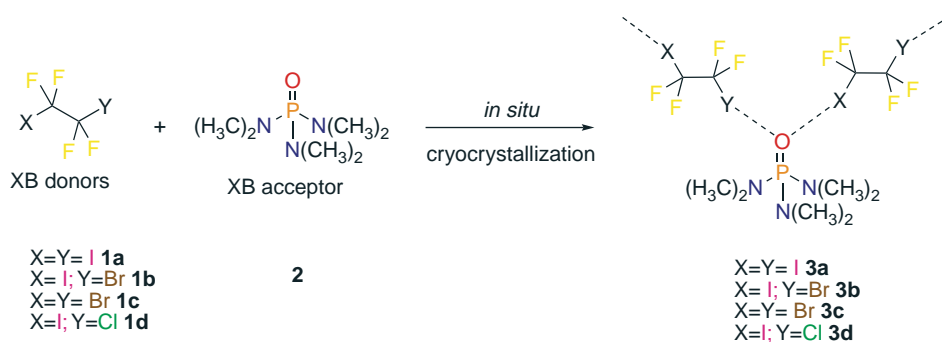
The exploitation of a lone pair on neutral atoms as XB acceptor site has allowed for the synthesis of a great variety of systems with quite different topologies (e.g. discrete adducts, one-, two- and three-dimensional networks with various connectivities) and unique and useful functional properties (4, 5) [e.g. liquid crystals (6), light-responsive polymers (7), NLO materials (8), low  $k$  conducting systems (9) and pharmaceutical cocrystals (10)].

A quite general and useful heuristic principle in the crystal engineering of halogen bonded supramolecular architectures involving neutral XB donors and acceptors requires the ‘one to one pairing’ between the lone pair on the XB acceptor atom (electron density donor site) and the positive  $\sigma$ -hole (11) on the halogen atom (electron

density acceptor site). The directionality of the entrance of the lone pair of the XB acceptor in the well-defined positive  $\sigma$ -hole of the XB donor allows for translating the molecular geometry of the interacting modules into the geometry of the supramolecular adducts (12). When anionic species are used as XB acceptors (13), it becomes much more challenging to predict the stoichiometry and the geometry of the formed architectures. This problem of control is related to the electron cloud surrounding the anionic species, which is more diffuse, thus less directional, in anions than the lone pair on a heteroatom. This feature of anions causes that a given anion can work as mono-, bi-, ... polydentate XB acceptor as a result of a subtle balance of several factors, among others the nature and the structure of the cation and the XB donor, the possible inclusion in the crystal of solvent molecules, etc.

The XBs between neutral nitrogen atoms, either in aromatic or aliphatic systems (14) and iodo- or bromocarbons with strong electron withdrawing groups close by the halogen atom give rise to the particularly robust C–X··N supramolecular synthons. They have been frequently used in the crystal engineering of organic co-crystals. The C–X··O supramolecular synthons involving the XB donors mentioned earlier and a neutral oxygen atom as XB acceptor site have been investigated to a lesser extent (15) despite oxygen functionalities are quite common in organic compounds. In the Cambridge Structural Database (CSD) (16), the structures where the C–X··N synthons (X = Cl, Br or I) play a driving role in the components self-assembly are almost twice the

\*Corresponding authors. Email: [gabriella.cavallo@polimi.it](mailto:gabriella.cavallo@polimi.it); [giancarlo.terraneo@polimi.it](mailto:giancarlo.terraneo@polimi.it)



Scheme 1. (Colour online) Molecular formulae of starting tectons **1a–1d**, **2** and corresponding halogen bonded adducts **3a–3d**.

structures assembled, thanks to the C–X···O synthons (see Supplementary Information, available online).

C–X···O synthons, possibly in combination with hydrogen bonding (HB) based synthons, can be used to create and control the structure of new supramolecular entities of potential relevance to many fields, spanning from materials chemistry to biopharmacology (17). It thus becomes important to gain further information on these synthons and this is particularly true for the poorly known C–Cl···O synthon. We thus undertook a research project aimed at deepening our knowledge on such synthons and assess their role in affecting, or determining, the packing of crystalline solids. We have already reported a study of the C–Br···O synthon, in which the cryocrystallisation technique was used to analyse the low melting adducts formed by some commonly used solvents containing a carbonyl, sulphonyl or phosphoryl moiety and a liquid dibromoperfluoroarene (18). Here, we describe how the same crystallisation technique can be used to investigate the analogous low melting adducts **3a–3d** formed by the dihaloperfluoroalkanes **1a–1d** with hexamethylphosphor-triamide (**2**, HMPA) (Scheme 1).

The adopted technique is powerful enough to give information not only on the moderately strong C–I···O synthon, but also on the weaker C–Br···O synthon, and even on the much weaker C–Cl···O synthon. Thermal and infrared (IR) analyses as well as computational studies of **3a–3d** consistently support conclusions from crystallographic investigations and indicate that also the C–Cl···O synthon determines both the structural features of heteromeric crystals and their stoichiometry.

Tectons **1a–1d** and **2** have been selected to maximise the possibility to obtain neat and detailed evidences on the C–X···O synthons and their role in promoting self-assembly processes. Crystallography being a key technique in our studies, it was important to maximise the possibility that the structural features of co-crystals **3a–3d** give reliable indications on the inherent features of C–X···O synthons. Tectons **1a–1d** and **2** have been selected as they minimise the possible formation of non-covalent interactions other than the C–X···O XBs under study. These

tectons allow for net contribution of C–X···O synthons to the self-assembly processes to be studied in conditions of synthon isolation. Moreover, a further advantage of halofluoroalkanes **1a–1d** is the fact that the respective heavy halogen atoms are particularly strong XB donors in their class. In fact, the high electronegativity of fluorine allows chloro-, bromo- and iodoperfluorocarbons to form with a given nucleophile, stronger XBs than hydrocarbon analogues. Similarly, HMPA **2**, a common organic solvent, has been preferred to other oxygenated solvents since its oxygen atom can function as strong XB acceptor (19), thanks to its particularly high electron density (18). Finally, with the aim to minimise the chance that the crystal packing under study is mainly controlled by space filling requirements, small tectons have been used, namely dihaloperfluoroethanes **1a–1d** have been preferred over longer chain analogues. Being quite minimal in the tectons used, the halogen-bonded adducts, **3b–3d**, are liquid at room temperature. To overcome this problem, the so-called *in situ* cryocrystallisation was used, as it allows the crystal growth from the liquid directly on the diffractometer by using an optical heating and crystallisation device (OHCD). During the years, this method has been successfully used to obtain structural information of unusual and new supramolecular systems formed, thanks to weak interactions (20).

## 2. Results and discussion

Differential scanning calorimetry (DSC) was used to determine the **1a–1d:2** pairing ratio optimal for obtaining a single heteromeric adduct and afforded preliminary information on the self-assembly process forming corresponding adducts **3a–3d**. Mixtures 1:1, 1:2 and 2:1 were examined and only the first ratio showed no residual peaks for the ‘excess’ starting material for all the four XB donors **1a–1d** both on cooling and heating scans. The oxygen atom of HMPA is known to function as bidentate XB acceptor (18, 19) and the observed optimal ratio being the same for the four tectons **1a–1d**, it seems that not only iodine, but also bromine and chlorine atoms in **1a–1d** work as XB donor sites. The four 1,2-dihalotetrafluoroethanes **1a–1d** all

seem to function as ditopic XB donors and the 1:1 tectons ratio was systematically used in all successive studies. A single peak was observed in the cooling ramp of 1:1 mixtures of **1a–1d** and **2**, suggesting the formation of single supramolecular adducts in all four cases.

The melting points of supramolecular architectures **3a–3c** are higher than those of corresponding pure fluorocarbon modules **1** and of pure hydrocarbon module **2**. The adduct **3a**, given by diiodotetrafluoroethane (**1a**, DITFE), exhibits the highest melting point of the series (90°C), the adducts **3b** and **3c**, formed by bromiodotetrafluoroethane (**1b**, BrITFE) and dibromotetrafluoroethane (**1c**, DBrTFE), melt at 28 and 14°C, respectively, and the adduct **3d**, given by chloriodotetrafluoroethane (**1d**, ClITFE), melts at –12°C. The trend shown by the melting points of adducts **3** parallels the expected XB donor ability of the heavy halogen atoms in tectons **1**. The heavier a halogen atom is, the stronger the XB it forms (*1*).

The melting point of a molecular solid is determined by a subtle balance of all packing forces inherent to its molecular components, nevertheless the observed trend in **3a–3d** suggests that XBs are not only present in the adducts but they are the strongest interactions in these systems and thus play a major role in determining their melting points. This hypothesis is confirmed by a comparison between the melting points of adducts **3** and the mean value of the melting points of the starting tectons **1** and **2**. This type of comparison allowed for filing a ranking of different XBs which is similar to the rankings based on other approaches (*21*). The adduct **3a**, wherein two strong C–I··O XBs are expectedly present per starting tecton unit, melts 97°C higher than the mean value of starting tectons (melting points: **3a**, 90°C; **1a**, –21°C and **2**, 7°C; mean value, –7°C) while **3c**, wherein two weak C–Br··O XBs are expectedly present, melts 65°C higher than the mean value of starting tectons (melting points: **3c**, 14°C; **1c**, –110°C and **2**, 7°C; mean value, –51°C).

IR spectra of adducts **3** are approximately the sum of the spectra of single tectons **1** and **2** but some minor band shifts support the possible presence of XBs. The  $\nu_{\text{P=O}}$  stretching band of pure HMPA **2** is at 1210 cm<sup>–1</sup> in the gas phase and is red shifted whenever the oxygen atom interacts with electron density acceptor sites (e.g. on HB formation and metal coordination). It is at 1202 cm<sup>–1</sup> in the pure and liquid HMPA, where weak HBs are present (*18*), and it is at 1192 cm<sup>–1</sup> in the diiodide adduct **3a**, at 1197 cm<sup>–1</sup> in the monoiodides **3b** and **3d** and at 1199 cm<sup>–1</sup> in the dibromide **3c**. These values suggest that HMPA oxygen atoms in **3a–3d** interact with stronger electron density acceptor sites than in pure HMPA, consistent with the presence of XBs in both solid and liquid 1:1 mixtures of starting tectons **1** and **2**. Interestingly, the stronger the XBs in adducts **3** are (expected strength scale **3a** > **3b** ~ **3d** > **3c**), the greater the redshifts are relative to pure HMPA.

X-ray studies gave detailed structural information on all four supramolecular complexes **3a–3d** and confirmed the presence and the importance of C–X··O XBs. Crystals of **3b** (BrITFE/HMPA), **3c** (DBrTFE/HMPA) and **3d** (ClITFE/HMPA) suitable for single crystal X-ray analysis were formed by using the *in situ* cryocrystallisation method and employing an OHCD. Several cycles of partial melting and re-crystallisation of the 1:1 mixtures of starting tectons were required, and both the temperature and the speed (time) of the crystal growth process were optimised (see Experimental section). Good quality single crystals were obtained at 285, 220 and 200 K for **3b**, **3c** and **3d**, respectively, in good agreement with DSC data. The crystal structure of **3a** (DITFE/HMPA), which is solid at room temperature, is already known (*19*); however, the low quality of reported X-ray data prompted us to re-collect the diffraction data (on a sample obtained through isothermal crystallisation from a dichloromethane solution) in order to get better structural information of the C–I··O synthon.

All the four co-crystals **3** are isostructural, crystallise in the *P2<sub>1</sub>/c* space group (Table 1) and contain **1** and **2** in a 1:1 ratio. The change of some features at the molecular level, with respect to the pure components, is consistent with IR differences between the pure components and their co-crystals. The P=O bond length in **3a–3d** is slightly elongated (0.010–0.018 Å) with respect to the pure **2** in agreement with the IR shift to lower wavenumbers of the  $\nu_{\text{P=O}}$  stretching band in the co-crystal with respect to pure **2**.

The supramolecular arrangement of the four co-crystals **3** is mainly controlled by XBs between the oxygen atom of HMPA **2** and the activated I, Br and Cl atoms of **1a–1d** (Figure 1).

Both the XB donor and acceptor tectons, **1a–1d** and **2**, respectively, behave as bidentate modules and infinite chain, propagating along the crystallography *b*-axis, is formed wherein **1a–1d** and **2** alternate (Figure 2).  $\alpha,\omega$ -Dihaloperfluoroalkanes typically adopt an *all-trans* conformation and the two C–X bonds are nearly parallel; moreover, the two lone pairs on the oxygen atom of HMPA adopt an angled arrangement. The XB directionality (*22*) translates these geometrical features of starting tectons **1** and **2** into the geometrical features of the self-assembled architecture **3**, and the halogen-bonded infinite chains adopt an undulated shape wherein HMPA imposes the angulation and dihalotetrafluoroethanes work as linear spacers of bending sites.

Perfluorocarbon and hydrocarbon moieties typically have a low reciprocal affinity (*23*). As reminiscent of this low affinity, a clear segregation is present in the overall architecture of the co-crystals **3a–3d** wherein the two tectons form columnar arrangements (Figure 3). Weak HBs occurring between the halogen atoms (mainly fluorine) in **1a–1d** and the hydrogen atoms in **2** interconnect the halogen-bonded chains.

Table 1. Crystal data and structure refinement parameters for **3a–3d**.

Compound	<b>3a<sup>a</sup></b>	<b>3b<sup>b</sup></b>	<b>3c<sup>b</sup></b>	<b>3d<sup>b</sup></b>
Formula	C <sub>8</sub> H <sub>18</sub> N <sub>3</sub> PO F <sub>4</sub> I <sub>2</sub>	C <sub>8</sub> H <sub>18</sub> N <sub>3</sub> PO F <sub>4</sub> I Br	C <sub>8</sub> H <sub>18</sub> N <sub>3</sub> PO F <sub>4</sub> Br <sub>2</sub>	C <sub>8</sub> H <sub>18</sub> N <sub>3</sub> PO F <sub>4</sub> ICl
<i>M<sub>r</sub></i>	533.02	486.03	439.04	441.57
Space group	<i>P</i> 2 <sub>1</sub> / <i>c</i>	<i>P</i> 2 <sub>1</sub> / <i>c</i>	<i>P</i> 2 <sub>1</sub> / <i>c</i>	<i>P</i> 2 <sub>1</sub> / <i>c</i>
Crystal system	Monoclinic	Monoclinic	Monoclinic	Monoclinic
<i>a</i> (Å)	7.0037(19)	6.9605(10)	6.8796(5)	6.9456(5)
<i>b</i> (Å)	16.447(4)	16.304(2)	16.1759(12)	16.2499(13)
<i>c</i> (Å)	14.853(4)	14.743(2)	14.5360(9)	14.7351(12)
β (°)	101.761(13)	102.225(5)	102.812(3)	102.516(4)
<i>V</i> (Å <sup>−3</sup> )	1675.0(8)	1635.2(4)	1577.35(19)	1623.6(2)
<i>Z</i>	4	4	4	4
<i>D</i> <sub>calc</sub> (g cm <sup>−3</sup> )	2.114	1.947	1.849	1.807
F(0 0 0)	1008.0	936	864	864.0
λ (Å)	Mo Kα/0.71073	Mo Kα/0.71073	Mo Kα/0.71073	Mo Kα/0.71073
Temperature (K)	100	100	100	100
μ (Mo Kα)/mm <sup>−1</sup>	3.886	4.535	5.277	2.271
θ range (°)	1.87–26.00	1.89–26.00	2.52–33.22	2.51–26.00
No. of reflections	40,915	19,075	14,358	59,600
<i>R</i> <sub>int</sub>	0.0328	0.0892	0.1609	0.0721
<i>R</i> <sub>σ</sub>	0.0143	0.0576	0.1106	0.0284
No. of ref. Par.	178	202	178	208
<i>R</i> ( <i>I</i> > 2σ( <i>I</i> ))	0.0138	0.0655	0.0446	0.0264
<i>wR</i> ( <i>F</i> <sup>2</sup> )( <i>I</i> > 2σ( <i>I</i> ))	0.0338	0.1931	0.1085	0.0596
Goodness of fit, <i>S</i>	1.224	1.070	1.014	1.151
Residual peaks (eÅ <sup>−3</sup> )	−0.473/0.337	−1.497/5.312	−0.848/1.07	−0.369/0.953
CCDC	941,383	941,386	941,384	941,385

<sup>a</sup> Isothermal crystallisation at room temperature from dichloromethane.

<sup>b</sup> *In situ* cryocrystallisation, using OHCD system.

C–I···O XBs in complexes **3a**, **3b** and **3d** are remarkably short and directional (Table 2), namely the interatomic attractive force is particularly strong, probably thanks to the good electron donor ability of the oxygen atom of HMPA (18, 24). The I···O normalised contacts ( $N_c$  is the ratio  $D_{ij}/(\text{rvd}W_i + \text{rvd}W_j)$ , where  $D_{ij}$  is the distance between the atoms *i* and *j* and  $\text{rvd}W_i$  and  $\text{rvd}W_j$  are the van der Waals radii for atoms *i* and *j*, respectively.) are ~0.80 if atoms are assumed to be spherical and Bondi's (25) van der Waals radii are used (I, 1.98 Å; O, 1.52 Å). These contacts are shorter than expected even if iodine atoms are assumed to be ellipsoidal and Nyburg and Fearman's value (26) is used for the smaller van der Waals radius (1.76 Å,  $N_c = 0.86$ ). Consistent with the C–I···O interaction strength, these XBs are able to replace completely the HB framework present in the crystal structure of pure **2** and this is the case also in **3c** where only the weaker C–Br···O interactions are present. A statistical analysis of the CSD reveals that the heavier the halogen atom is, the closer to linearity the XBs which it forms are (1). Consistent with this trend, the observed C–Br···O and C–Cl···O angles are less linear than C–I···O angles and interaction distances correspond to smaller normalised contacts (Table 2), suggesting weaker interactions. Nevertheless in these cases too,  $N_c$  values lower than 1.00, namely atoms interpenetration, are

observed if ellipsoidal shape is assumed for the halogen atoms and Nyburg and Fearman's value are used.

The fluorinated tectons **1b** and **1d** in adducts **3b** and **3d** show some disorder which has been modelled considering that the space between two successive HMPA molecules **2** in a halogen-bonded infinite chain is occupied by molecules X–CF<sub>2</sub>CF<sub>2</sub>–I (X = Br, Cl) disordered in two orientations (i.e. I–CF<sub>2</sub>CF<sub>2</sub>–X or X–CF<sub>2</sub>CF<sub>2</sub>–I) (27). These two molecules have the same conformations, are slightly translated from each other along the longest molecular axis and populate the space between two successive HMPA molecules with a site occupancy factor of 0.5. As a result of this orientational disorder, all atoms are splitted over two positions occupied by the same element but the terminal heavy halogen atoms, which exchange each other. This static disorder is probably due to the comparable surface electrostatic potential and steric hindrance of I, Br and Cl atoms (28).

The mapping of the electrostatic potential ( $V(\mathbf{r})$ ) distribution (0.001 e/bohr<sup>3</sup> charge density isosurface) around the XB donor and acceptor modules **1** and **2** affords useful rationalisation of the observed intermolecular interactions. The oxygen atom of **2** has the most negative area (blue colour in Figure 4), perfectly consistent with its functioning as the only XB acceptor site. The heavier halogen atoms in the perfluorinated



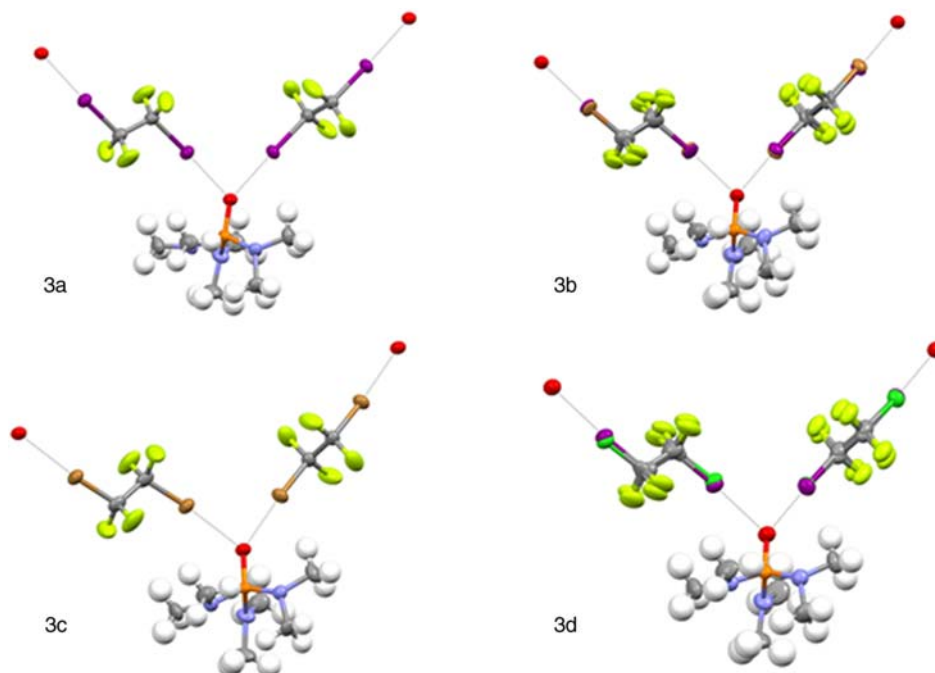


Figure 1. (Colour online) Ellipsoid representation (85% probability) for a trimeric motif in **3a–3d**. XBs are black dotted lines. In **3b** and **3d**, all atoms of **1b** and **1d** tectons are splitted over two positions (possibly with different colours) corresponding to the two orientations these tectons adopt in the co-crystals. Colour code: carbon, dark grey; hydrogen, light grey; oxygen, red; nitrogen, sky blue; fluorine, yellow; phosphors, orange; iodine, purple; bromine, brown and chlorine, green.

tectons **1a–1d** show a remarkably anisotropic electron distribution accounting for their ‘amphoteric’ character. A positive electrostatic potential (i.e. the  $\sigma$ -hole responsible for the XB donor behaviour, yellow/red colour in Figure 4) is along the direction of the C–X covalent bond, while a belt-shaped surface orthogonal to the covalent bond has a negative potential (nucleophilic character, blue colour). The calculated  $V_{s,max}$  values parallel the common trend of XB donor ability ( $I > Br > Cl$ ) and, for a given halogen atom, slightly

change with the overall electron withdrawing ability of the residue it is bound to. Differently, fluorine atoms in **1a–1d** show a nearly uniform negative potential as, in general, this halogen displays a positive  $\sigma$ -hole, and functions as electrophile (29), only when bound to an exceptionally strong electron withdrawing group.

The natural bond orbital (NBO) analysis can assign the percentage of  $s$ - and  $p$ -character of a given orbital and when performed on **1a–1d** (adopting the conformation observed in **3a–3d**) confirms that fluorine atoms are

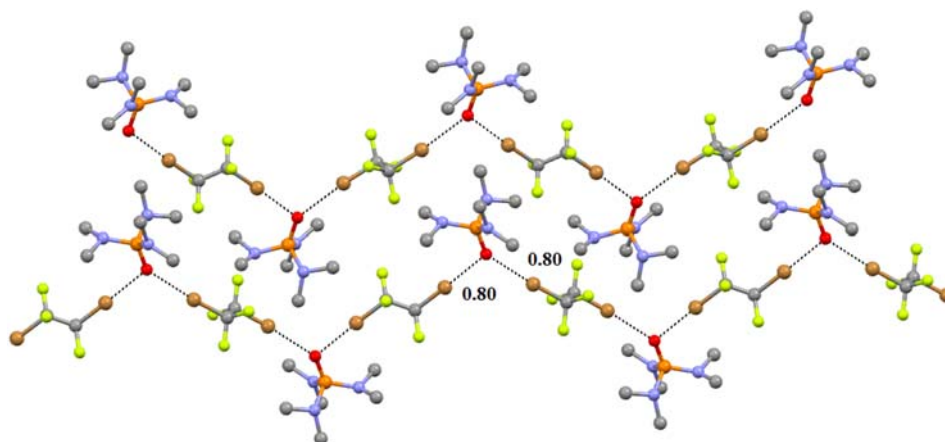


Figure 2. (Colour online) Ellipsoid representation for the halogen bonded infinite supramolecular chains for **3c**. Halogen bonds are black dotted lines and digits are  $N_c$  values for C–Br $\cdots$ O XBs. Colour code as in Figure 1.

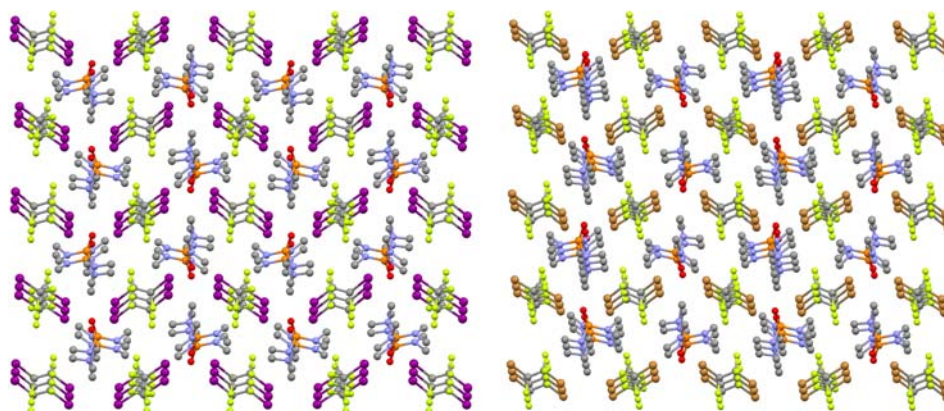


Figure 3. (Colour online) Ball and stick representation of the crystal packing for **3a** (left) and **3c** (right) wherein the two tectons segregate in a columnar shape. Hydrogen atoms are omitted for clarity. Colour as in Figure 1.

tailored to work as electron density donors rather than acceptors (Table 3).

In **1a–1d**, each halogen atom is involved in a C–X bonding orbital,  $\sigma_{CX}$ , and has three unshared electron pairs, of which two of them are perpendicular to the C–X axis while the third one is along the C–X bond axis. In our systems, this latter electron lone pair has more than 90% *s*-character for iodine, bromine and chlorine atoms but only 70% for fluorine. Differently, the contribution of each halogen atom to the  $\sigma_{CX}$  bonding is mainly a *p*-orbital, the *s*-character for fluorine atoms being more than twice those of chlorine, bromine and iodine atoms. NBO analysis also reveals that there is a significant shift of the bonding electron density towards the fluorine atom, the share being 70% for fluorine compared to  $\sim 45\%$  for other halogens. The combination of the high halogen population character in the bonding electrons  $\sigma_{CX}$  (fluorine is the most electronegative element) and the relatively large *p*-character for the unshared *s*-electron pairs, neutralises the  $\sigma$ -hole on the fluorine atom leaving it completely negative. As reported by Clark and Politzer (30), fluorine

atom has a much greater *sp*-hybridisation than the heavier halogens and this character is also observed in **1a–1d**. The *s*-character of bonding orbitals slightly increases from I in **1a** to Br in **1c**, parallel to the *p*-character of the unshared electrons. This is the reason why the magnitude of the area with positive electrostatic potential varies with the halogen atom, I atom presenting a larger and more positive  $\sigma$ -hole than Br and Cl (Figure 4). Mulliken charges calculation

Table 2. C–X...O distances, normalised contacts ( $N_c$ ) and C–X...O angles  $\theta$  in **3a–3d**.

	C–X...Y	X...O (Å)	$N_c^a$	$\theta$ (°)
<b>3a</b>	C1–I1...O1	2.801(2)	0.80	175.53
	C2–I2...O1	2.814(1)	0.80	177.00
<b>3b</b>	C1–I1...O1	2.7909(2)	0.80	174.25
	C3–I2...O1	2.8114(2)	0.80	174.82
<b>3c</b>	C2–Br1...O1	2.8494(2)	0.85	174.05
	C4–Br2...O1	2.7761(2)	0.83	171.23
<b>3d</b>	C1–Br1...O1	2.811(3)	0.83	175.3
	C2–Br2...O1	2.811(3)	0.83	175.1
<b>3d</b>	C1–I1...O1	2.7742(1)	0.79	176.54
	C3–I2...O1	2.7586(2)	0.79	176.16
	C2–Cl1...O1	2.9294(2)	0.90	172.45
	C4–Cl2...O1	2.8958(2)	0.88	171.20

<sup>a</sup> Calculated by using Bondi's van der Waals radii (25): Cl, 1.76 Å; Br, 1.85 Å; I, 1.98 Å; O, 1.52 Å.

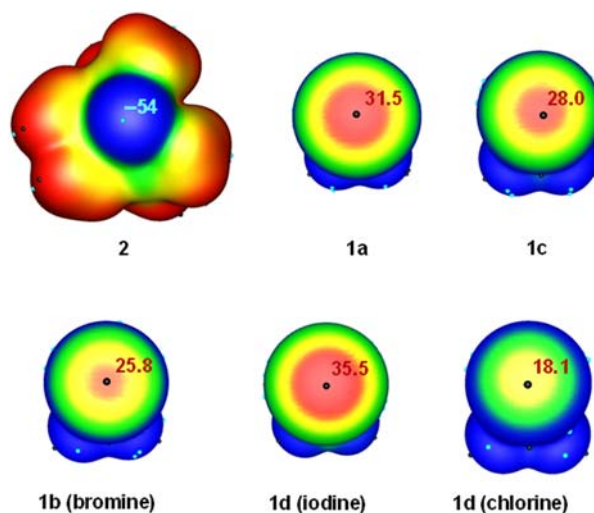


Figure 4. (Colour online) Electrostatic potential ( $\text{kcal mol}^{-1}$ ) computed on  $0.001 \text{ e/bohr}^3$  charge density isosurface of HMPA **2** (top left), DITFE **1a** (top mid), DBrTFE **1c** (top right), BrITFE **1b** (bottom left, bromine in front), ClITFE **1d** (bottom mid, iodine in front) and ClITFE **1d** (bottom right, chlorine in front). The colour ranges for the halogen-bonding acceptor **2** are as follows: red more positive than  $-1.49$ ,  $-1.49 > \text{yellow} > -18.84$ ,  $-18.84 > \text{green} > -36.19$  and blue less than  $-36.19$ ; the colour ranges for the dihaloperfluoroalkanes **1a–1d** are as follows: red more positive than  $22.00$ ,  $22.00 > \text{yellow} > 13.00$ ,  $13.00 > \text{green} > 3.50$  and blue less than  $3.50$ . The  $V_s(\mathbf{r})$  critical points are superimposed to the surface: Black points are the maxima of electrostatic potential, values are given in dark red; the light blue points are the minima, value is given in sky blue.

Table 3. NBO population analysis for XCF<sub>2</sub>CF<sub>2</sub>Y (X and Y as in Scheme 1).

Compound	X, Y and F	Halogen population in the $\sigma_{cx}$ -NBO (%)	$\sigma_{cx}$ (NBO)		Unshared s-electron pair (NBO)	
			s (%)	p (%)	s (%)	p (%)
<b>1a</b>	I	41.85	6.99	92.83	93.09	6.90
	$\langle F \rangle^a$	71.29	28.36	72.51	70.17	29.76
<b>1b</b>	I	38.69	7.695	92.15	92.615	7.35
	Br	49.655	7.475	92.165	92.335	7.665
<b>1c</b>	$\langle F \rangle^a$	70.87	27.46	72.41	71.26	28.74
	Br	47.37	9.25	90.43	90.92	9.07
<b>1d</b>	$\langle F \rangle^a$	71.05	28.60	71.26	70.47	29.52
	I	38.275	7.97	91.875	92.49	7.5
	Cl	53.035	10.795	88.775	89.405	10.595
	$\langle F \rangle^a$	70.805	27.65	72.21	71.29	28.7

<sup>a</sup> Average value for the four fluorine atoms.

and atomic natural charges obtained from NBO analysis performed on **1a–1d** also support the absence of the  $\sigma$ -hole on fluorine atoms (Table S1, available online).

Computational studies on the experimental geometry of the trimeric motif of **3a** and **3c** where two molecules of XB donors **1** are bound to one molecule of **2** also provide useful information on the C–I $\cdots$ O and C–Br $\cdots$ O interactions. The binding energy for the two XBs formed by an oxygen atom is 7.90 kcal mol<sup>-1</sup> for **3a** and 5.46 kcal mol<sup>-1</sup> for **3c**. These values are similar to those calculated for similar interactions involving haloperfluoroaromatics (18) and show the same trend of the potential of the positive  $\sigma$ -hole on the halogen atom and of the melting points of co-crystals **3** (measured *via* DSC).

Single point calculation on the crystal structure of **2** allows to establish that the binding energy of a dimer in the pure compound (1.08 kcal mol<sup>-1</sup>), which measures the strength of the HB network in pure **2**, is smaller than binding energies of heteromeric co-crystals **3a** and **3c**. The higher stability of O $\cdots$ X interactions over O $\cdots$ H ones justifies the preferential growth of heteromeric and halogen bonded complexes **3** over the formation of the homomeric and hydrogen bonded crystal of pure **2**.

### 3. Conclusions

In this paper, we assessed the ability of C–X $\cdots$ O supramolecular synthons (X = I, Br and Cl) to promote molecular recognition and self-assembly processes. The structurally simple tectons **1a–1d** and **2** have been used with the aim to minimise the presence of supramolecular synthons different from those under study and to avoid the relevance of space filling requirements in determining the overall crystal packing of the formed heteromeric adducts **3a–3d**. Experimental evidences supported by computational studies reveal how the C–X $\cdots$ O synthons are able to completely substitute for the C–H $\cdots$ O synthon present in the crystal structure of pure **2** and to drive the formation

of the isostructural architectures **3a–3d**. The good quality of the single crystals used in the X-ray diffraction experiments prove the effectiveness of the *in situ* cryocrystallisation technique using an OHCD and its remarkable potential in the study of the weak interactions present in systems which are liquid at room temperature and pressure. HMPA is confirmed to be a particularly good oxygen-centred XB acceptor molecule; the C–Cl $\cdots$ O synthon, while weaker than the C–Br $\cdots$ O and C–I $\cdots$ O analogues, seems to be able not only to affect, but also to determine the structure and the composition of a heteromeric adduct. The C–X $\cdots$ O synthon is confirmed a valuable tool in supramolecular chemistry and its exploitation may impact different fields such as the design of solid functional materials and the molecular recognition of biological molecules and macromolecules (17). This paper provides further knowledge in the field of ‘weak’ intermolecular interactions, a clue in both chemical and biological sciences.

## 4. Experimental

### 4.1 Samples preparation

1,1-Diiodotetrafluoroethane (**1a**), 1-bromo-2-iodotetrafluoroethane (**1b**), 1,2-dibromotetrafluoroethane (**1c**), 1-chloro-2-iodotetrafluoroethane (**1d**) and hexamethylphosphorotriamide (**2**) were purchased from commercial companies and used without further purification (Sigma-Aldrich, Milan, Italy and FluoroChem, Hadfield, UK). Screening of XB donor and XB acceptor ratio has been done in order to obtain the desired co-crystals. In all the co-crystals **3a–3d**, the optimal XB donor:XB acceptor ratio is 1:1. Sonication was applied for 10 min to all the liquid mixtures to improve the mixing. Single crystals of **3a** suitable for X-ray analysis were obtained *via* recrystallisation of poorly crystalline violet powder obtained from dichloromethane. The co-crystals **3b**, **3c** and **3d** were obtained by *in situ* cryocrystallisation.



#### 4.2 DSC and IR data collection

DSC analyses were performed using a Mettler Toledo DSC 823e (Mettler Toledo, Novate Milanese, Italy) to determine the correct stoichiometries of the adducts between **1** and **2** and to obtain the melting points of the complexes for the following *in situ* cryocrystallisation. The starting compounds and their liquid mixtures were first cooled to  $-50^{\circ}\text{C}$  ( $3^{\circ}\text{C}/\text{min}$ ) then heated up at the same rate. For the solid compound **3a**, a heating scan method was used instead (heating up to  $100^{\circ}\text{C}$  at  $3^{\circ}\text{C}/\text{min}$  and then cooling to room temperature). IR spectra were obtained using a Nicolet Nexus FTIR spectrometer (Nicolet Nexus, Thermo Fisher Scientific, Milan, Italy) equipment with attenuated total reflectance (ATR) device. Selected bands that provide some preliminary evidences about halogen bond formation are given in the Results and discussion section. DSC plots and IR spectra are reported in Supplementary Information, available online.

#### 4.3 In situ cryocrystallisation procedure

The liquid mixtures of **3b**, **3c** and **3d** were sealed in 0.3 mm borosilicate glass capillaries of 2 cm length. The capillaries were fixed on a standard goniometer head and mounted on a Bruker KAPPA APEX II diffractometer (Bruker A.X.S., Milan, Italy) equipped with a Bruker KRYOFLEX low temperature device ( $\text{N}_2$  stream) and an OHCD (31) for the *in situ* cryocrystallisation. The crystals of **3b**, **3c** and **3d** were obtained at 285, 220 and 200 K, respectively, in good agreement with the preliminary DSC results. Several cycles of partial melting and re-crystallisation of the samples, according to prof. Boese's protocol, were performed by varying temperature and time; they were important in order to achieve the formation of a good single crystal.

#### 4.4 Single crystal X-ray diffraction experiments

A suitable crystal obtained at room temperature for **3a** and crystals grown *in situ* for **3b**, **3c** and **3d** were analysed on a Bruker KAPPA APEX II diffractometer with a CCD detector and using a monochromatic  $\text{Mo K}\alpha$  radiation source, operating at 50 kV and 40 mA. X-ray diffraction data were collected at low temperature (100 K) for all crystals, in order to improve data quality, using both  $\omega$  and  $\phi$  scans with a scan width of  $0.5^{\circ}$ . The detector distance was set to 40 mm to the samples. The data collection and reduction were done using SMART software. The empirical absorption correction was applied. All structures were solved by direct methods and refined by full-matrix least-square on  $F^2$  using SHELX-97 package (32). During structures solution and refinement, all atoms (except H) have been refined anisotropically; the positions of the hydrogen atoms have been placed through geometrical considerations.

The molecular and crystal packing diagrams were generated using Mercury (33). Geometrical calculations were done using PARST95 (34) present in the WinGX program suite (35). Hirshfeld surfaces were computed with CrystalExplorer 2.1 (36) in order to analyse intermolecular interactions in the experimental crystal structures. Further details about data collections and refinements are reported in Table 1.

#### 4.5 Computational details

Detailed information on electron density distribution, electrostatic potential ( $V(\mathbf{r})$ ), binding energy and charge analysis for the halogen bonded co-crystals were obtained by single point calculations on the experimental geometries performed at the B3LYP/DZVP level of theory, using Gaussian09 code (37). All electron basis sets were used for all atoms. The quality of the functional and of the basis sets used was tested comparing the results, especially from the binding energy calculation, with previous works on XB. The data reported are referred to the best combination of basis sets method, obtained after several trials. For co-crystals **3a** and **3c**, the interaction energies were computed and opportunely corrected for the basis sets superposition errors using the well-known counterpoise correction (38). The electrostatic potential on charge density isosurfaces of the trimers was computed, using the  $0.001 \text{ e}/\text{bohr}^3$  ( $0.0067 \text{ e}/\text{\AA}^3$ ) contour of the electron density as previously suggested by Bader (39). The WFA software (40) developed by Politzer et al. was used to perform the topological analysis of electrostatic potential on the halogen bonded co-crystals.

#### Supplementary Information

CSD analysis, DSC thermograms and FTIR spectra, Mulliken and NBO charges analysis, extra figures and check-cif files for **3a–3d** are available in the Supplementary Information.

#### Acknowledgements

The authors gratefully acknowledge the financial support from MIUR (project PRIN 2010–2011, Nos 2010CX2TLM\_004 and 2010ERFKXL 005).

#### References

- (1) (a) Beale, T.M.; Chudzinski, M.G.; Sarwar, M.G.; Taylor, M.S. *Chem. Soc. Rev.* **2013**, *42*, 1667–1680. (b) Politzer, P.; Murray, J.S. *ChemPhysChem.* **2013**, *14*, 278–294. (c) Metrangolo, P.; Resnati, G. *Cryst. Growth Des.* **2012**, *12*, 5835–5838. (d) Erdélyi, M. *Chem. Soc. Rev.* **2012**, *41*, 3547–3557. (e) Parisini, E.; Metrangolo, P.; Pilati, T.; Resnati, G.; Terraneo, G. *Chem. Soc. Rev.* **2011**, *40*, 2267–2278. (f) Cavallo, G.; Metrangolo, P.; Pilati, T.; Resnati, G.; Sansotera, M.; Terraneo, G. *Chem. Soc. Rev.* **2010**, *39*,

- 3772–3783. (g) Bertani, R.; Sgarbossa, P.; Venzo, A.; Lelj, F.; Amati, M.; Resnati, G.; Pilati, T.; Metrangolo, P.; Terraneo, G. *Coord. Chem. Rev.* **2010**, *254*, 677–695. (h) Rissanen, K. *CrystEngComm* **2010**, *10*, 1107–1113.
- (2) Desiraju, G.R.; Ho, P.S.; Kloo, L.; Legon, A.C.; Marquardt, R.; Metrangolo, P.; Politzer, P.; Resnati, G.; Rissanen, K. *Pure Appl. Chem.* **2013**, *85*. doi: 10.1351/PAC-REC-12-05-10.
- (3) Politzer, P.; Murray, J.S.; Clark, T. *Phys. Chem. Chem. Phys.* **2013**, *15*, 11178–11189.
- (4) (a) Metrangolo, P.; Neukirch, H.; Pilati, T.; Resnati, G. *Acc. Chem. Res.* **2005**, *38*, 386–395. (b) Priimagi, A.; Cavallo, G.; Metrangolo, P.; Resnati, G. *Acc. Chem. Res.* **2013**, *46*. doi: 10.1021/ar400103r.
- (5) (a) Meazza, L.; Foster, J.A.; Fucke, K.; Metrangolo, P.; Resnati, G.; Steed, J.W. *Nat. Chem.* **2013**, *5*, 42–47. (b) Jentzsch, A.V.; Emery, D.; Mareda, J.; Nayak, S.K.; Metrangolo, P.; Resnati, G.; Sakai, N.; Matile, S. *Nat. Commun.* **2012**, *3*, art. no. 905. (c) Meyer, F.; Dubois, P. *CrystEngComm* **2013**, *15*, 3058–3071.
- (6) (a) Bertani, R.; Metrangolo, P.; Moiana, A.; Perez, E.; Pilati, T.; Resnati, G.; Rico-Lattes, I.; Sassi, A. *Adv. Mater.* **2002**, *14*, 1197–1201. (b) Bruce, D.W.; Metrangolo, P.; Meyer, F.; Präsang, C.; Resnati, G.; Terraneo, G.; Whitwood, A.C. *New J. Chem.* **2008**, *32*, 477–482. (c) Präsang, C.; Nguyen, H. L.; Horton, P.N.; Whitwood, A.C.; Bruce, D.W. *Chem. Commun.* **2008**, 6164–6166. (d) Bruce, D.W.; Metrangolo, P.; Meyer, F.; Pilati, T.; Präsang, C.; Resnati, G.; Terraneo, G.; Wainwright, S.G.; Whitwood, A. C. *Chem. Eur. J.* **2010**, *16*, 9511–9524.
- (7) (a) Priimagi, A.; Cavallo, G.; Forni, A.; Gorynsztejn-Leben, M.; Kaivola, M.; Metrangolo, P.; Milani, R.; Shishido, A.; Pilati, T.; Resnati, G.; Terraneo, G. *Adv. Funct. Mater.* **2012**, *22*, 2572–2579. (b) Priimagi, A.; Saccone, M.; Cavallo, G.; Shishido, A.; Pilati, T.; Metrangolo, P.; Resnati, G. *Adv. Mater.* **2012**, *24*, OP345–OP352.
- (8) (a) Cariati, E.; Forni, A.; Biella, S.; Metrangolo, P.; Meyer, F.; Resnati, G.; Righetto, S.; Tordin, E.; Ugo, R. *Chem. Commun.* **2007**, 2590–2592. (b) Cariati, E.; Cavallo, G.; Forni, A.; Leem, G.; Metrangolo, P.; Meyer, F.; Resnati, G.; Righetto, S.; Terraneo, G.; Tordin, E. *Cryst. Growth Des.* **2011**, *11*, 5642–5648.
- (9) Sgarbossa, P.; Bertani, R.; Di Noto, V.; Piga, M.; Giffin, G.A.; Terraneo, G.; Pilati, T.; Metrangolo, P.; Resnati, G. *Cryst. Growth Des.* **2012**, *12*, 297–305.
- (10) Baldrighi, M.; Cavallo, G.; Chierotti, M.R.; Gobetto, R.; Metrangolo, P.; Pilati, T.; Resnati, G.; Terraneo, G. *Mol. Pharm.* **2013**, *10*, 1760–1772.
- (11) (a) Riley, K.E.; Murray, J.S.; Concha, M.C.; Hobza, P.; Politzer, P. *J. Chem. Theory Comput.* **2009**, *5*, 155–163. (b) Politzer, P.; Murray, J.S.; Clark, T. *Phys. Chem. Chem. Phys.* **2010**, *12*, 7748–7757.
- (12) (a) Metrangolo, P.; Meyer, F.; Pilati, T.; Resnati, G.; Terraneo, G. *Angew. Chem. Int. Ed.* **2008**, *47*, 6114–6127. (b) Biella, S.; Gattuso, G.; Notti, A.; Metrangolo, P.; Pappalardo, S.; Parisi, M.F.; Pilati, T.; Resnati, G.; Terraneo, G. *Supramol. Chem.* **2009**, *21*, 149–156.
- (13) (a) Cametti, M.; Raatikainen, K.; Metrangolo, P.; Pilati, T.; Terraneo, G.; Resnati, G. *Org. Biomol. Chem.* **2012**, *10*, 1329–1333. (b) Martí-Rujas, J.; Colombo, L.; Lü, J.; Dey, A.; Terraneo, G.; Metrangolo, P.; Pilati, T.; Resnati, G. *Chem. Commun.* **2012**, 8207–8209. (d) Kilah, N.L.; Wise, M.D.; Serpell, C.J.; Thompson, A.L.; White, N.G.; Christensen, K. E.; Beer, P.D. *J. Am. Chem. Soc.* **2010**, *132*, 11893–11895. (e) Metrangolo, P.; Pilati, T.; Terraneo, G.; Biella, S.; Resnati, G. *CrystEngComm* **2009**, *11*, 1187–1196.
- (14) (a) Biella, S.; Cametti, M.; Caronna, T.; Cavallo, G.; Forni, A.; Metrangolo, P.; Pilati, T.; Resnati, G.; Terraneo, G. *Supramol. Chem.* **2011**, *23*, 256–262. (b) Crihfield, A.; Hartwell, J.; Phelps, D.; Walsh, R.B.; Harris, J.L.; Payne, J.F.; Pennington, W.T.; Hanks, T.W. *Cryst. Growth Des.* **2003**, *3*, 313–320. (c) Neukirch, H.; Guido, E.; Liantonio, R.; Metrangolo, P.; Pilati, T.; Resnati, G. *Chem. Commun.* **2005**, 1534–1536. (d) Metrangolo, P.; Meyer, F.; Pilati, T.; Proserpio, D.M.; Resnati, G. *Chem. Eur. J.* **2007**, *13*, 5765–5772.
- (15) (a) Eccles, K.S.; Morrison, R.E.; Stokes, S.P.; O’Mahony, G.E.; Hayes, J.A.; Kelly, D.M.; O’Boyle, N.M.; Fábíán, L.; Moynihan, H.A.; Maguire, A.R.; Lawrence, S.E. *Cryst. Growth Des.* **2012**, *12*, 2969–2977. (b) Hanson, G.R.; Jensen, P.; McMurtrie, J.; Rintoul, L.; Micallef, A.S. *Chem. Eur. J.* **2009**, *15*, 4156–4164. (c) Gajda, R.; Katrusiak, A.; Crassous, J. *CrystEngComm* **2009**, *11*, 2668–2676.
- (16) Allen, F.H. *Acta Crystallogr.* **2002**, *B58*, 380–388.
- (17) (a) Bolton, O.; Lee, K.; Kim, H.-J.; Lin, K. Y.; Kim, J. *Nat. Chem.* **2011**, *3*, 205–210; (b) Carter, M.; Ho, P.S. *Cryst. Growth Des.* **2011**, *11*, 5087.
- (18) Nayak, S.N.; Terraneo, G.; Forni, A.; Metrangolo, M.; Resnati, G. *CrystEngComm* **2012**, *14*, 4259–4261.
- (19) Chu, Q.; Wang, Z.; Huang, Q.; Yan, C.; Zhu, S. *New J. Chem.* **2003**, *27*, 1522–1527.
- (20) (a) Kirchner, M.T.; Blaser, D.; Boese, R. *Chem. Eur. J.* **2010**, *16*, 2131–2146. (b) Boese, R.; Blaser, D.; Jansen, G.J. *Am. Chem. Soc.* **2009**, *131*, 2104–2106. (c) Boese, R.; Kirchner, M.T.; Billups, W.E.; Norman, L.R. *Angew. Chem. Int. Ed.* **2003**, *42*, 1961–1963. (d) Dikundwar, A.G.; Sathishkumar, R.; Guru Row, T.N.; Desiraju, G.R. *Cryst. Growth Des.* **2011**, *11*, 3954–3963. (e) Nayak, S.K.; Sathishkumar, R.; Guru Row, T.N. *CrystEngComm* **2010**, *12*, 3112–3118. (f) Nayak, S.K.; Prathapa, S.J.; Guru Row, T.N. *J. Mol. Struct.* **2009**, *935*, 156–162. (g) Choudhury, A.R.; Winterton, N.; Steiner, A.; Cooper, A. I.; Johnson, K.A. *J. Am. Chem. Soc.* **2005**, *127*, 16792–16793. (h) Yufit, D.S.; Howard, J.A.K. *CrystEngComm* **2010**, *12*, 737–741.
- (21) De Santis, A.; Forni, A.; Liantonio, R.; Metrangolo, P.; Pilati, T.; Resnati, G. *Chem. Eur. J.* **2003**, *9*, 3974–3983.
- (22) Saccone, M.; Cavallo, G.; Metrangolo, P.; Pace, A.; Pibiri, I.; Pilati, T.; Resnati, G.; Terraneo, G. *CrystEngComm* **2013**, *15*, 3102–3105.
- (23) (a) Rocaboy, C.; Hampel, F.; Gladysz, J.A. *J. Org. Chem.* **2002**, *67*, 6863–6870. (b) Navarrini, W.; Metrangolo, P.; Pilati, T.; Resnati, G. *New J. Chem.* **2000**, *24*, 777–780.
- (24) (a) Messina, M.T.; Metrangolo, P.; Panzeri, W.; Ragg, E.; Resnati, G. *Tetrahedron Lett.* **1998**, *39*, 9069–9072. (b) Metrangolo, P.; Panzeri, W.; Recupero, F.; Resnati, G. *J. Fluorine Chem.* **2002**, *144*, 27–33.
- (25) (a) Bondi, A. *J. Phys. Chem.* **1964**, *68*, 441–451. (b) Bondi, A. *Physical Properties of Molecular Crystals, Liquids and Glasses*, John Wiley: New York, 1968, p. 450ff.
- (26) Nyburg, S.C.; Faerman, C.H. *Acta Crystallogr.* **1985**, *B41*, 274–279.
- (27) Olejniczak, A.; Katrusiak, A.; Vij, A. *CrystEngComm* **2009**, *11*, 1073–1080.
- (28) Olejniczak, A.; Katrusiak, A.; Vij, A. *CrystEngComm* **2009**, *11*, 1240–1244.
- (29) (a) Metrangolo, P.; Murray, J.S.; Pilati, T.; Politzer, P.; Resnati, G.; Terraneo, G. *CrystEngComm* **2011**, *13*, 6593–6596. (b) Metrangolo, P.; Murray, J.S.; Pilati, T.; Politzer, P.; Resnati, G.; Terraneo, G. *Cryst. Growth Des.* **2011**, *11*, 4238–4246.

- (30) (a) Clark, T.; Hennemann, M.; Murray, J.S.; Politzer, P. *J. Mol. Model.* **2007**, *13*, 291–296. (b) Politzer, P.; Lane, P.; Concha, M.C.; Ma, Y.; Murray, J.S. *J. Mol. Model.* **2007**, *13*, 305–311 and reference therein.
- (31) <http://www.sci-ohcd.eu/>.
- (32) Sheldrick, G.M. *Acta Crystallogr.* **2008**, *A64*, 112–122.
- (33) Macrae, C.F.; Bruno, I.J.; Christolm, P.R.; Edgington, P.R.; McCabe, P.; Pidcock, E.; Rodriguez-Monge, L.; Taylor, R.; van de Steek, J.; Wood, P.A. *J. Appl. Crystallogr.* **2008**, *41*, 466–470. <http://www.ccdc.cam.ac.uk/mercury/>.
- (34) Nardelli, M.J. *J. Appl. Crystallogr.* **1995**, *28*, 659–673.
- (35) Farrugia, L.J. *J. Appl. Crystallogr.* **1999**, *32*, 837–838, *WINGX* (ver. 1.80.05).
- (36) CrystalExplorer 2.1 (381), Wolff, S.K.; Grimwood, D.J.; McKinnon, J.J.; Jayatilaka, D.; Spackman, M.A. (2005–2007) University of Western Australia; <http://hirshfeldsurface.net/CrystalExplorer/>.
- (37) Frisch, M.J.; Trucks, G.W.; Schlegel, H.B.; Scuseria, G.E.; Robb, M.A.; Cheeseman, J.R.; Scalmani, G.; Barone, V.; Mennucci, B.; Petersson, G.A.; Nakatsuji, H.; Caricato, M.; Li, X.; Hratchian, H.P.; Izmaylov, A.F.; Bloino, J.; Zheng, G.; Sonnenberg, J.L.; Hada, M.; Ehara, M.; Toyota, K.; Fukuda, R.; Hasegawa, J.; Ishida, M.; Nakajima, T.; Honda, Y.; Kitao, O.; Nakai, H.; Vreven, T.; Montgomery, J.A., Jr.; Peralta, J.E.; Ogliaro, F.; Bearpark, M.; Heyd, J.J.; Brothers, E.; Kudin, K.N.; Staroverov, V.N.; Kobayashi, R.; Normand, J.; Raghavachari, K.; Rendell, A.; Burant, J.C.; Iyengar, S.S.; Tomasi, J.; Cossi, M.; Rega, N.; Millam, J. M.; Klene, M.; Knox, J.E.; Cross, J.B.; Bakken, V.; Adamo, C.; Jaramillo, J.; Gomperts, R.; Stratmann, R.E.; Yazyev, O.; Austin, A.J.; Cammi, R.; Pomelli, C.; Ochterski, J.W.; Martin, R.L.; Morokuma, K.; Zakrzewski, V.G.; Voth, G.A.; Salvador, P.; Dannenberg, J.J.; Dapprich, S.; Daniels, A.D.; Farkas, Ö.; Foresman, J. B.; Ortiz, J. V.; Cioslowski, J.; Fox, D.J. *Gaussian 09*; Gaussian, Inc.: Wallingford CT, 2009.
- (38) Boys, S.F.; Bernardi, F. *Mol. Phys.* **1970**, *19*, 553–566.
- (39) Bader, R.F.W.; Carrol, M.T.; Cheeseman, J.R.; Chang, C. *J. Am. Chem. Soc.* **1987**, *109*, 7968–7979.
- (40) Bulat, F.A.; Toro-Labbe, A.; Brink, T.; Murray, J.S.; Politzer, P. *J. Mol. Model.* **2010**, *16*, 1679–1691.